Geomorphology 335 (2019) 62–75

Contents lists available at ScienceDirect

Geomorphology

journal homepage: www.elsevier.com/locate/geomorph

Combination of GNSS, satellite InSAR, and GBInSAR remote sensing monitoring to improve the understanding of a large landslide in high alpine environment

Tommaso Carlà [a,*], Veronica Tofani [a], Luca Lombardi [a], Federico Raspini [a], Silvia Bianchini [a], Davide Bertolo [b], Patrick Thuegaz [b], Nicola Casagli [a]

[a] University of Florence, Department of Earth Sciences, Via La Pira 4, 50121 Firenze, Italy
[b] Dipartimento Programmazione, Difesa del Suolo e Risorse Idriche, Regione Autonoma Valle d'Aosta, Loc. Amérique 33, 11020 Quart, Aosta, Italy

ARTICLE INFO

Article history:
Received 13 July 2018
Received in revised form 4 March 2019
Accepted 15 March 2019
Available online 22 March 2019

Keywords:
Slope monitoring
Large alpine landslides
Sentinel-1
GBInSAR

ABSTRACT

The investigation of large landslides in high alpine environments is often hindered by the difficult accessibility of the mountainous terrain. Efforts are typically concentrated on the remote measurement of the surface displacements, in order to define the general slope dynamics and identify phases of increasing activity. The characterization of such phenomena is challenging, due to their complex nature as well as the limitations of monitoring techniques. Appropriately integrating monitoring data from different sources can help reduce uncertainties, yet it is seldom done. In this paper, the outcomes of GNSS, satellite InSAR, and GBInSAR campaigns performed at the Bosmatto landslide (Northwestern Alps, Italy) are presented. The joint analysis provided a comprehensive view of the deformation field of the landslide, which revealed a gradually decreasing dip angle of the calculated movement vectors from head to toe. The instability was interpreted as a $2.5 - 3.5 * 10^6$ m^3 rockslide, moving at peak velocities >50 mm/y according to a broadly roto-translational mechanism. The impact of the seasonal snow cover on the reliability of the interferometric acquisitions was also evaluated. Advantages and implications offered by the combination of multiple monitoring techniques are highlighted.

1. Introduction

Large landslides in steep alpine slopes are a considerable threat to vulnerable communities and infrastructures. Their destructive power is related to their potential to undergo rapid accelerations and evolve into catastrophic rock avalanches, which expose valley bottoms to exceptional risks (Crosta et al., 2017). An accurate characterization of these phenomena requires a thorough understanding of the predisposing geological factors, controlling factors, and failure mechanism. In this regard, the possibility to perform detailed in situ investigations and geotechnical surveys is heavily constrained by logistical and/or economical limitations, owing to the typically rough, vast, and remote terrain. Stabilization works are impractical to undertake for the same reasons, and because they cannot be engineered based on ground-proof data. Furthermore, large landslides in steep alpine slopes are frequently complex, to the point that separate individual sectors may be present and behave differently within the instability. The activity and sensitivity to perturbations may also be variable across the slope (Crosta et al., 2014).

Remediation and early warning strategies are commonly centered on the continuous monitoring of the slope displacements, which can give crucial information on the dynamics and evolution of the landslide (Eberhardt et al., 2008). Several cases of displacement monitoring of large landslides in alpine areas have been reported (Barla et al., 2010; Casagli et al., 2010; Gaffet et al., 2010; Nishii and Matsuoka, 2010; Gischig et al., 2011; Del Ventisette et al., 2012; Marcato et al., 2012; Crosta et al., 2017). Each monitoring technique, taken individually, has limitations, and as a result a dense and/or multiparameter data coverage is often difficult to obtain (Helmstetter and Garambois, 2010). For instance, measurements from conventional monitoring techniques (e.g. inclinometers, extensometers, topographic and GNSS surveying) are restricted only to a small number of ground points; laser-scanning applications are subject to extensive times of data processing; other advanced remote sensing techniques (e.g. ground-based and satellite interferometry) detect only a single component of the true movement vector of the slope. The various challenges that are inherent to monitoring in high alpine environments are then enhanced by the presence of a deep snow cover for prolonged periods of time each year.

Integrating data from different sources can help overcome these issues and derive properties of the phenomenon that would otherwise remain unknown. Surprisingly, only few attempts of such have been presented in the recent literature. Notable examples can be found in Barla et al. (2010),

* Corresponding author.
E-mail address: tommaso.carla@unifi.it (T. Carlà).

https://doi.org/10.1016/j.geomorph.2019.03.014

where the displacements measured by a ground-based interferometric radar over a large landslide in the Alps have been cross-validated with the displacements of four total station targets; Journalt et al. (2018) compared satellite interferometric measurements with GPS and ShapeAccelArray data to address the extent and magnitude of slope movements at the Ripley landslide (British Columbia, Canada); Bardi et al. (2014) combined ground-based and satellite interferometry to refine the precision of landslide mapping procedures; Carlà et al. (2018) combined ground-based and satellite interferometry to evaluate the precursors to an unpredicted slope failure in an open-pit mine; finally, Crosta et al. (2014) jointly analyzed borehole, GPS, optical targets, and ground-based interferometric radar data to extrapolate the relationship between the movements of the La Saxe rockslide (Italian Alps) and the seasonal snow melting.

In this paper, data acquired by three remote sensing monitoring systems over the Bosmatto landslide (Northwestern Alps, Italy) are presented (see Fig. 1 for the temporal coverage of each dataset). Specifically, these include:

- 3 and a half years of readings at two permanent GNSS (Global Navigation Satellite System) stations;
- 13 years of readings at five GNSS stations for campaign measurements (i.e. manually operated);
- 3 and a half years of InSAR (Interferometric Synthetic Aperture Radar) acquisitions from the Sentinel-1 satellite constellation (in both ascending and descending orbit).
- 8 months of measurements from a GBInSAR (Ground-Based Interferometric Synthetic Aperture Radar);

Coupled with geomorphological observations and with the stratigraphic profile from a borehole survey, the integration of the three datasets provided a comprehensive view of the deformation field of the landslide, and made it possible to infer key features concerning its mechanism and behavior. The impact of the snow cover on the reliability of the satellite InSAR and GBInSAR data was also assessed. The work highlights advantages and implications that combining monitoring data from different sources can offer to improve the understanding of large landslides in hardly accessible alpine slopes.

2. Description of the case study

The Bosmatto landslide is an ancient, large instability in a steep (30° to 40°) West-facing slope in the Northwestern Alps, overhanging the roughly N-S trending glacial Lys Valley above the village of Gressoney Saint-Jean (Aosta Valley, Italy). The complicated geological setting of this sector of the Lys Valley belongs to the Sesia-Lanzo Zone, which in turn is part of the Austroalpine domain in the Western Italian Alps.

The Sesia-Lanzo Zone consists of two elements: an upper element termed Second Diorito-Kinzigitic Zone, composed of pre-Alpine amphibolite-facies micaschists; a lower element, further subdivided into two metamorphic complexes named Gneiss Minuti Complex and Eclogitic Micaschists Complex (Dal Piaz et al., 1972; Compagnoni et al., 1977; Zucali et al., 2002). The Gneiss Minuti Complex consists of metagranitoids and minor metapelites with a dominant Alpine metamorphic imprint under greenschist facies conditions, whereas the Eclogitic Micaschists Complex mostly consists of metagranitoids, metapelites, and metabasites showing a dominant Alpine imprint under eclogite-facies conditions (Gosso, 1977; Zucali and Spalla, 2011). The instability falls entirely within a small sheet of the Eclogitic Micaschists Complex ("Punta Plaida Eclogitic Micaschists") that locally overlies the Second Diorito-Kinzigitic Zone, in proximity of the contact between these two formations (Fig. 2).

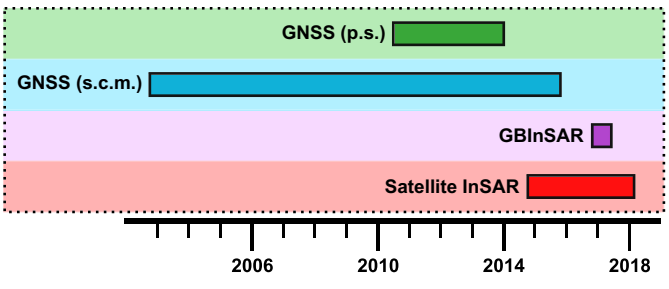

Fig. 1. Temporal coverage of the datasets used in this study. p.s. = permanent stations; s.c.m. = stations for campaign measurements.

The characteristics and evolution of the Bosmatto landslide are not well understood. The slope is split in two sectors with different state of activity: the southern inactive sector is completely vegetated by a dense high forest; the northern active sector (the one meant here as the "Bosmatto landslide"), extending longitudinally for at least 500 m and with a maximum width of approximately 300 m, lacks vegetation cover and appears as a highly chaotic mass of large disjointed blocks and fragments of metamorphic bedrock within a scarce sandy to gravelly matrix (Fig. 3a). Relatively coherent portions of rock mass are also present within the main body. The lower part of the slope is undercut by the deeply incised bed of the Letze Creek.

The Bosmatto landslide experienced a sudden reactivation on 15 October 2000, when an intense and prolonged rainfall event (330 mm between 11 and 16 October 2000) triggered an approximately 150,000 m^3 debris flow, partly originating at its toe. The debris flow, channeled down the Letze Creek and able to transport blocks of massive size (up to 10 m^3), reached the valley bottom and caused widespread damages to properties and infrastructures. Concurrently with this event, a new head scarp suddenly formed in the upper part of the slope at about 2100 m a.s.l., with the consequent collapse of a small portion of overlying rock mass ("rock spur" in Fig. 3b) beyond which the older head scarp is located. Fig. 3c shows a photo of the October 2000 debris flow, while Fig. 3d illustrates, looking down from the head scarp area towards the valley bottom, the large blocks that form the bulk of the landslide body.

Further details on the geomorphological features of the study area are reported in the three-dimensional sketch in Fig. 4. In the head scarp area, and beyond the main landslide body up to an elevation of about 2300 m a.s.l., rocky outcrops are heavily fractured and show signs of possible deep-seated deformation. The transition from the toe of the landslide to the debris flow source area is outlined by a minor scarp at 1700 m a.s.l., also formed during the October 2000 event. Below this point, five springs mark the point after which the Letze Creek has a perennial water flow, whereas water flow in the bed incisions upslope is intermittent or ephemeral. This hints at the presence of a complex water circulation system below the ground surface, possibly influencing the stability of the slope. The Letze Creek banks are very steep and prone to local phenomena of superficial erosion.

It is not known whether the slope movements are solely associated with toe undercutting and shallow mobilization of the unstable mass, or if active deformation and shearing of the bedrock at depth is also involved. Because of the heterogeneity of the landslide material and the high degree of disintegration of the outcropping bedrock, the relationship between the two units is unclear. A single borehole survey has been performed, in proximity of the minor scarp at 1700 m a.s.l. (Fig. 2). This indicated a 30-m thick layer of landslide material, separated from the bedrock by a roughly 10-m thick heavily deformed and brecciated zone with silty-sandy gauge layers that may act as a preferential plane of weakness (Fig. 5). The bedrock in the bottom half of the log presents a variable degree of fracturing with occasional breccia and fault gauge layers, mostly found in the upper section close to the heavily deformed zone.

Definitive conclusions on the mechanism of the instability cannot be extrapolated based on these limited data. Fig. 6 portrays a tentative cross-section of the slope (see AA' trace in Fig. 2). This is intended for illustrative purposes, and does not reflect the actual failure mechanism of the landslide.

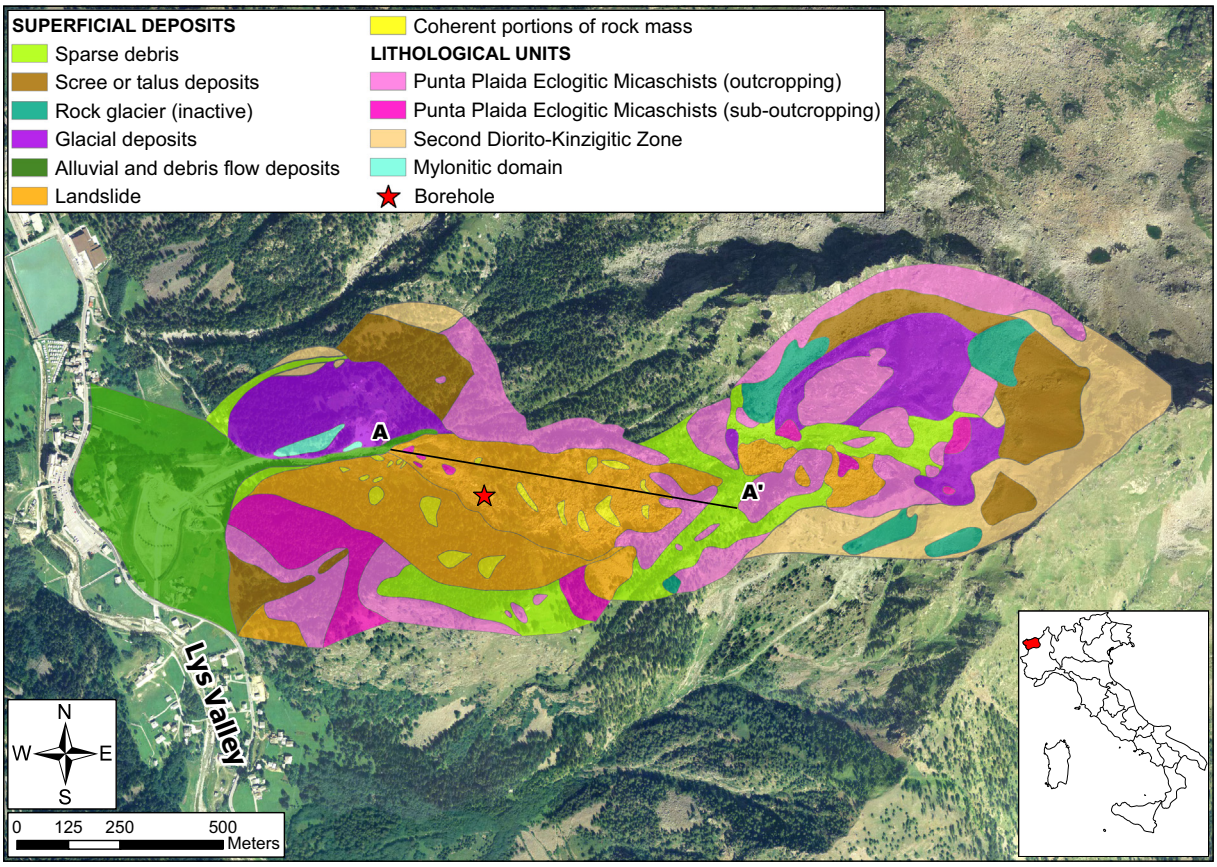

Fig. 2. Geological map of the study area. In the lower-right box, the Aosta Valley region is marked in red.

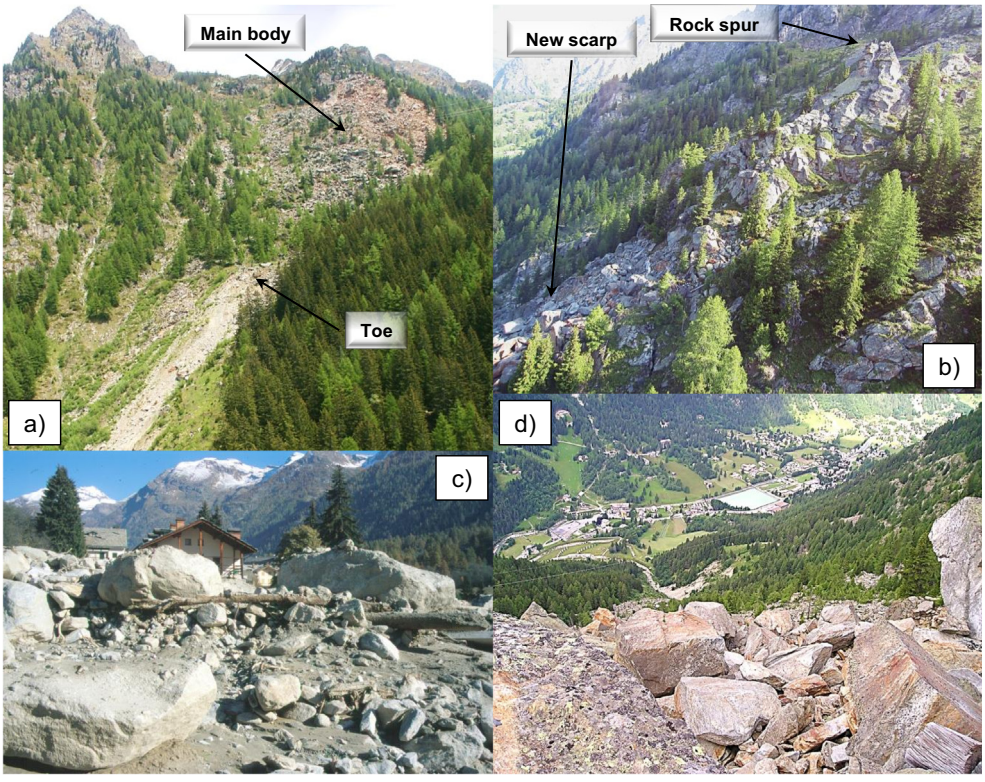

Fig. 3. Photos of the Bosmatto landslide: (a) frontal view of the landslide; (b) rock spur delimiting the head area; (c) October 2000 debris flow; (d) examples of large blocks that form the landslide body, looking down from the head area towards the valley bottom.

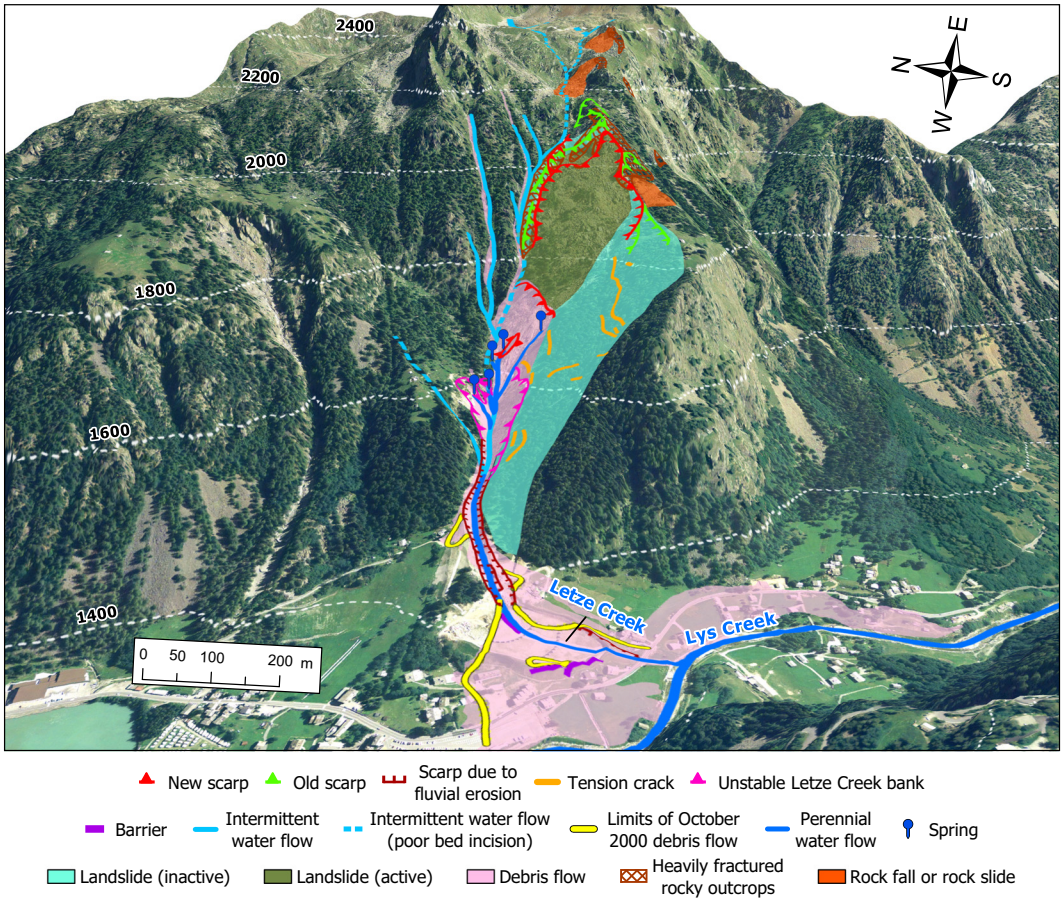

Fig. 4. Geomorphological map of the study area.

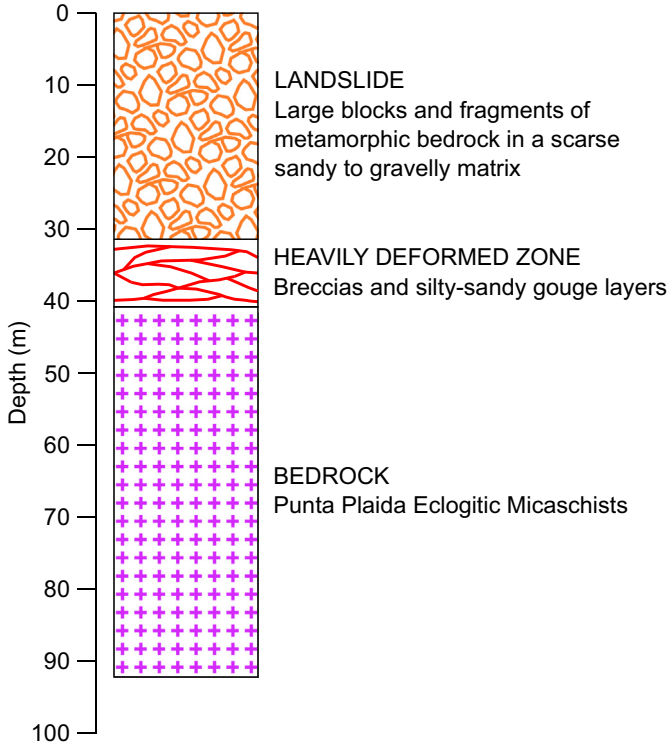

Fig. 5. Stratigraphic profile from the borehole indicated in Fig. 2.

3. Monitoring data

3.1. GNSS

A network of two permanent GNSS stations and five GNSS stations for campaign measurements was deployed on the landslide in the aftermath of the October 2000 reactivation (Fig. 7). Readings were made by means of dual-frequency static differential GNSS positioning. Antennas at permanent stations were installed on a pole and elevated at a height of 3 m above the ground in order to maintain clearance from the snow cover during the winter season; the available readings have a roughly 6-hour measurement frequency and span from 1 July 2010 to 31 December 2013. One of the two stations (A-05) was placed at the top of the new head scarp, while the other one (A-06) in proximity of the toe scarp. The stations for campaign measurements were materialized through rock-bolted threaded steel mounts, upon which to place the antenna. Readings were manually undertaken only once or twice a year (data from 3 October 2002 to 8 October 2015) because of the effort required to access the site and because of the impossibility to climb the mountain slope in presence of snow.

Fig. 7 highlights the average movement of each station in terms of vertical inclination (dip angle) and planimetric direction (azimuth) during the respective interval of monitoring. A mostly W-WNW movement of the landslide and a gradually decreasing dip angle from head to toe is observed. Figs. 8 and 9 indicate a generally constant rate of displacement, ranging from 8.6 mm/y (station A-05) to 74.8 mm/y (station M-08). In Fig. 8, data are also filtered according to a 50-point moving average, corresponding to a 12-day interval of acquisition.

The number of measurement points is still insufficient to interpret the kinematics of the slope at overall scale. Moreover, stations may report biased data if mounted on blocks resting in particularly unstable

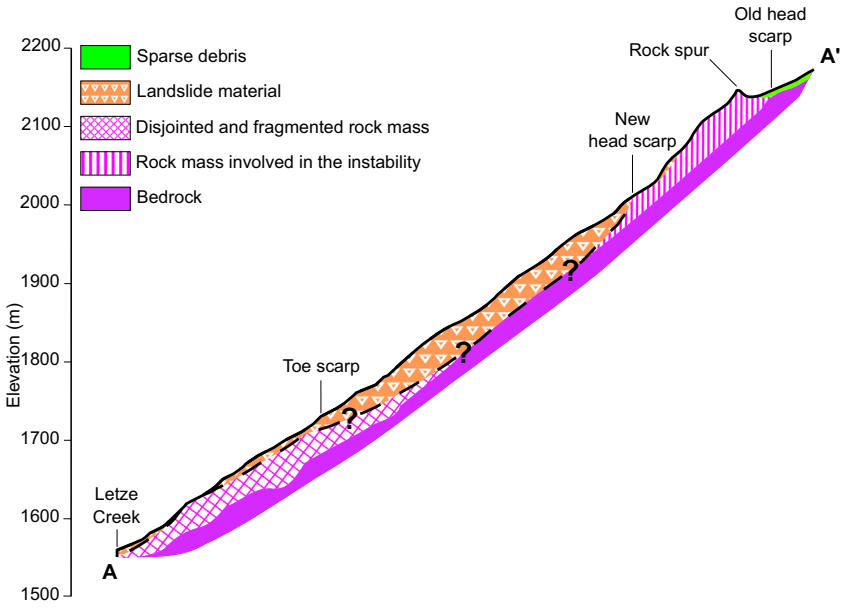

Fig. 6. Tentative slope cross-section (see AA' trace in Fig. 2).

positions and that are able to move with a higher degree of freedom. Such blocks may experience displacements that do not reflect the actual deformation of the slope. This aspect is difficult to determine in situ, given the chaotic nature of the landslide material.

Knowing the approximate 3D geometry of the slope surface deformation is essential for correcting InSAR-derived displacements. Radar interferometry can only capture the component of the displacement along the LOS (line-of-sight), that is the line connecting the target with the receiver. The cosine of the angle θ between the LOS versor and the slope movement versor defines the sensitivity of the sensor: $\cos\theta = 0$ means that no movement can be measured by the radar and $\cos\theta = 1$ means that the measured movement equals the real movement of the ground. The average dip angle and azimuth values of stations A-05 and A-06 (Fig. 7) have been taken, respectively, as representative of the slope movement versor at the head and toe of the landslide, and therefore to determine the sensitivity of the satellites and of the GBInSAR in these two sectors (see following Sections).

3.2. Satellite InSAR

Differential radar interferometry is a well-established active remote sensing technique that exploits the phase shift of the back-scattered electromagnetic wave between two or more coherent acquisitions. The recorded scene is arranged in a two-dimensional image and partitioned into pixels (Colesanti and Wasowski, 2006). A number of terms may merge into the returning phase values, among which contributions related to decorrelation, stereoscopic effects, and atmospheric artifacts. The working principle is based on isolating the phase term that is actually related to a variation of the sensor-to-ground path length, namely to a movement of the pixel.

Over the study area, the Sentinel-1 constellation acquired 130 IW (Interferometric Wide swath) scenes in descending orbit (satellite track 66), as well as further 130 IW scenes in ascending orbit (satellite track 88), from 10 October 2014 to 22 February 2018. The satellites operate in C-band (5.405 GHz) in the TOPS (Terrain Observation with

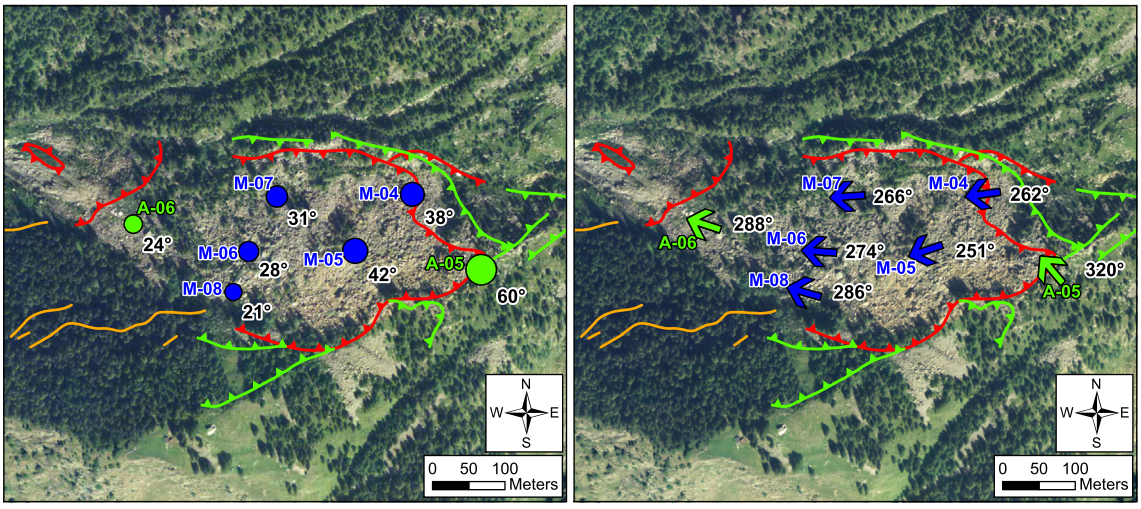

Fig. 7. Location of the GNSS stations, with average dip angle (left) and azimuth (right) of movement. Green markers represent permanent stations, blue markers stations for campaign measurements. See Fig. 4 for the meaning of the linear elements.

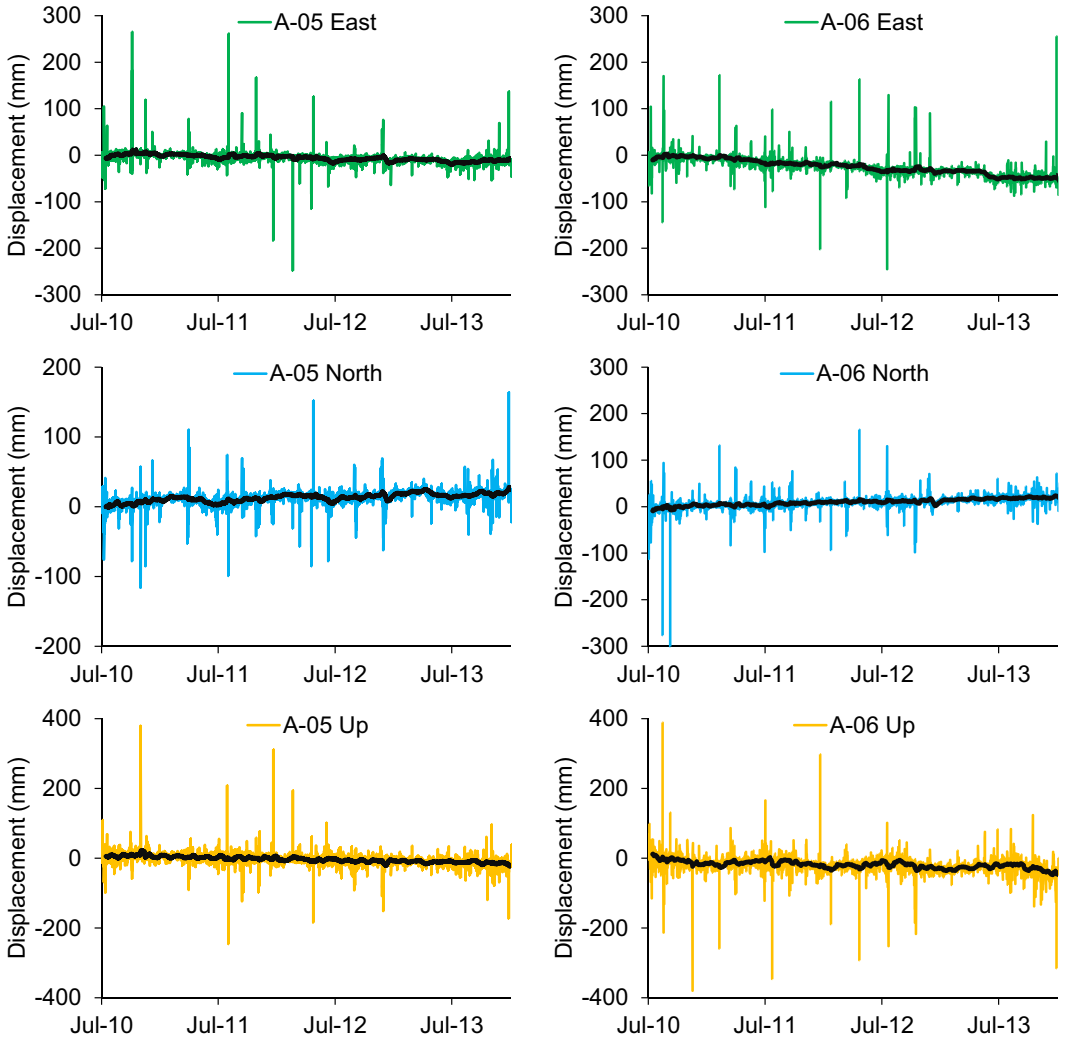

Fig. 8. Time series of displacement of the permanent GNSS stations. Black lines represent a 50-point moving average of the data.

Progressive Scans in azimuth) imaging mode. Launched in April 2014 and April 2016, Sentinel-1A and Sentinel-1B share the same orbital plane and offer an effective revisit time of 6 days (12 days for each sensor). For the dataset herein introduced, the 6-day revisit time has been available since early 2017. The InSAR products, featuring a spatial resolution of 4 × 14 m, were processed by means of the SqueeSAR algorithm, allowing for the identification of Persistent Scatterers (PS) and Distributed Scatterers (DS). PS are radar-bright and radar-phase stable pointwise targets with a dominant signal-to-noise ratio with respect to scene average, like rocky outcrops, roads, buildings, and other manmade objects; DS are statistically homogeneous groups of pixels sharing similar reflectivity and belonging to areas of moderate coherence like bare soil, debris fields, or non-cultivated land with short vegetation. Displacements are calculated relatively to a stable PS within the frame. A thorough description of the SqueeSAR processing steps is beyond the scope of this paper, and can be found in a reference work from Ferretti et al. (2011).

Figs. 10 and 11 display the resulting yearly LOS velocities in descending and ascending orbit, where negative values mean movement away from the sensor and positive values movement towards the sensor.

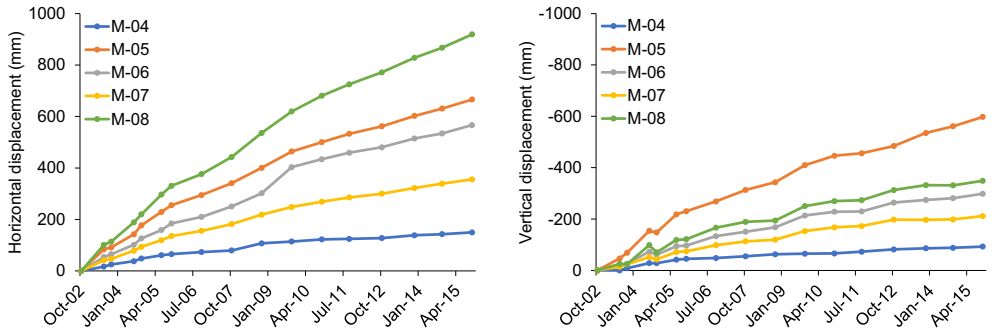

Fig. 9. Time series of displacement of the GNSS stations for campaign measurements.

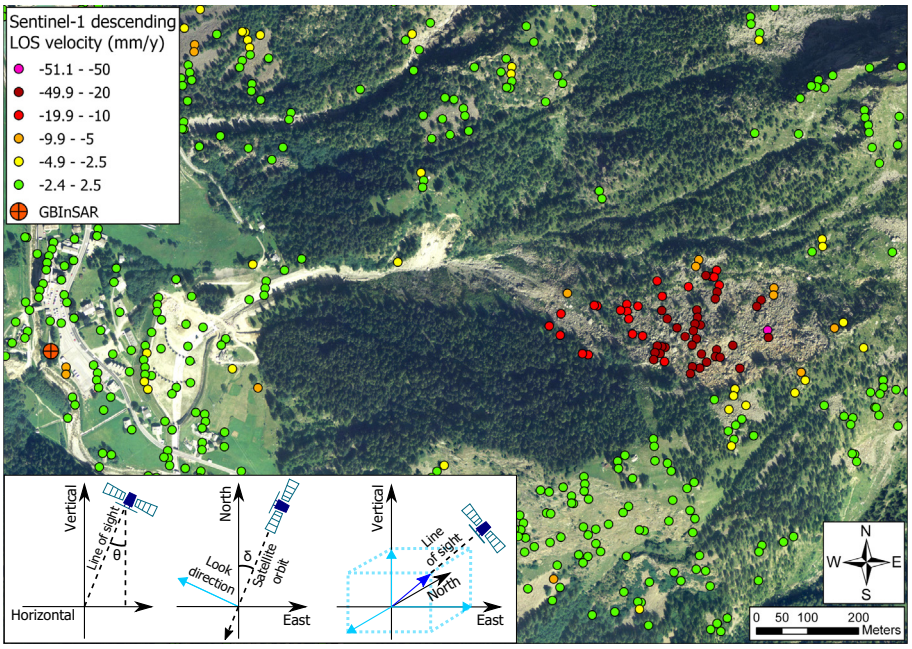

Fig. 10. Satellite InSAR data acquired in descending orbit over the study area.

Good spatial coverage was obtained over the landslide in both orbits. The two figures also show the position of the GBInSAR (see Section 3.3).

The LOS in descending orbit featured an incidence angle of 43.12° and a look direction of 280.49° N, broadly parallel to the dominant direction of movement of the main landslide body according to the GNSS records (Fig. 7). Acquisitions in descending orbit thus captured ~90% of the real movements in the head and toe area, and in general over the entire landslide. Accordingly, measured LOS velocities in Fig. 10 are consistent with the GNSS data (Fig. 8 and Fig. 9). The LOS in ascending orbit featured an incidence angle of 38.59° and a look direction of 81.13° N, almost perpendicular to the direction of slope movement. It follows that acquisitions in ascending orbit were nearly insensitive to the movements of the landslide along the horizontal component, hence the much lower LOS velocities in Fig. 11. Acquisitions in ascending orbit captured ~50% and ~20% of the real movements in the head and toe area, respectively. Most of the measured deformation is relative to the vertical component. The largest LOS velocities in ascending orbit were in fact measured in the head area, where vertical movements are more pronounced (Fig. 7). That is also the reason why several targets show negative velocities in spite of the slope moving planimetrically towards the sensor.

3.3. GBInSAR

A GBInSAR was deployed at the foot of the Letze Creek alluvial fan from 28 October 2016 to 30 June 2017 (position in Figs. 10 and 11). Based on the same physical principles of satellite InSAR, this technique has been proved suitable to landslide monitoring with minutely

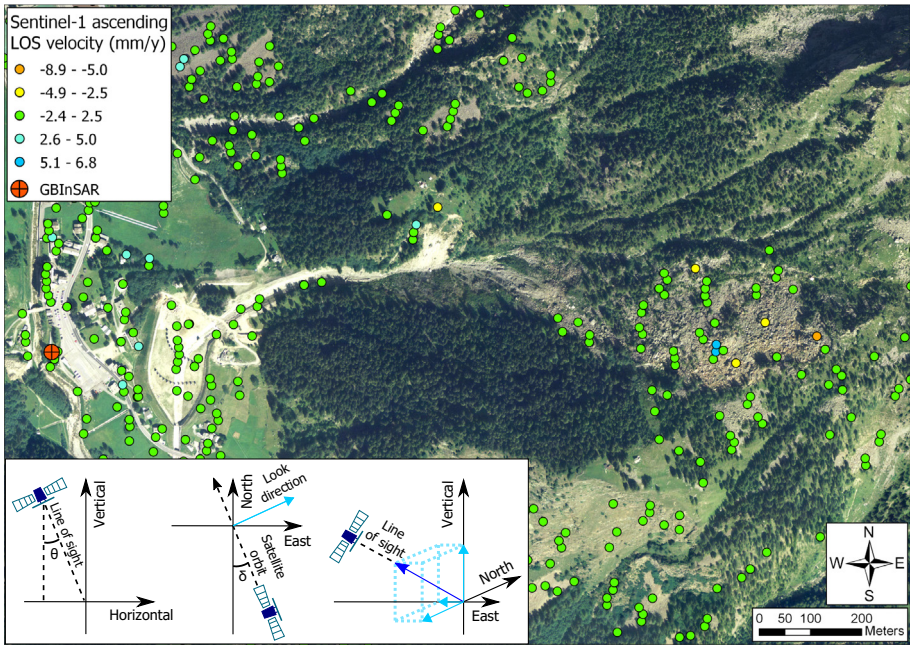

Fig. 11. Satellite InSAR data acquired in ascending orbit over the study area.

sampling rate and high spatial resolution (Leva et al., 2003; Tarchi et al., 2003; Antonello et al., 2004; Luzi et al., 2006; Casagli et al., 2010). The system operates in Ku-band (≈17 GHz) and is based on a continuous-wave step-frequency transmitter with a coherent receiver. The two antennas move with millimetric steps along a mechanical rail to form the synthetic aperture. Since the observational geometry is fixed, a zero-baseline configuration is attained. Atmospheric and instrumental decorrelation among different images is substantially reduced thanks to the higher acquisition frequency, allowing for the application of averaging and specific statistical tools (Luzi et al., 2004). The installation of artificial reflectors on the slope is not required, even in the poor visibility conditions typical of the winter season in high alpine environments.

Fig. 12 depicts the cumulative deformation map produced by the GBInSAR in the entire period of acquisition. During the monitoring campaign, control points inside and outside the boundaries of the landslide were extracted in order to survey in near real-time the displacement time series of selected sectors of the deformation map. Control points 11–14 were placed at the transition between the toe of the landslide and the debris flow source area, where the instrument has a sensitivity of ~90%; control points 07–09 were instead placed in the head scarp area, where the instrument, because of the larger elevation difference between the sensor and the target, has a sensitivity of ~65%.

While the largest displacements were rightfully detected within the boundaries of the landslide, the dataset is somewhat inconsistent with respect to the GNSS and satellite InSAR records. Despite the moderate LOS sensitivity, the head scarp area moves at a considerably larger average rate according to the GBInSAR (up to 70 mm of LOS displacement during the 8 months of acquisition, Fig. 12). Correcting the displacements according to a 65% LOS sensitivity would yield a velocity of the head scarp area of about 160 mm/y, more than doubling the GNSS and satellite InSAR records in the same area (Figs. 8–10). Significant movements were also unexpectedly detected in other sectors of the radar deformation map. For example, an alignment of pixels affected by relatively large values of displacement overlaps the Letze Creek bed incision in the higher portion of the slope. This cannot be associated with any reasonable process of ground deformation, and suggests that the GBInSAR data were affected by some sort of bias in phase of acquisition or processing.

4. Analysis and discussion

The three datasets have different characteristics and modes of acquisition. None of them alone is able to give conclusive information concerning the mechanism and behavior of the Bosmatto landslide. Furthermore, some uncertainties arise from their inconsistency with each other. The role played by the snow cover in determining data bias and the definition of the probable mechanism of the landslide are hereby addressed.

4.1. Influence of the snow cover

Even if ground-based and satellite radar interferometry have found extensive application for the monitoring of unstable slopes in alpine areas (Strozzi et al., 2005; Colesanti and Wasowski, 2006; Casagli et al., 2010; Crosta et al., 2014; Tessari et al., 2017; Manconi et al., 2018), little attention has been given to the influence that the prolonged

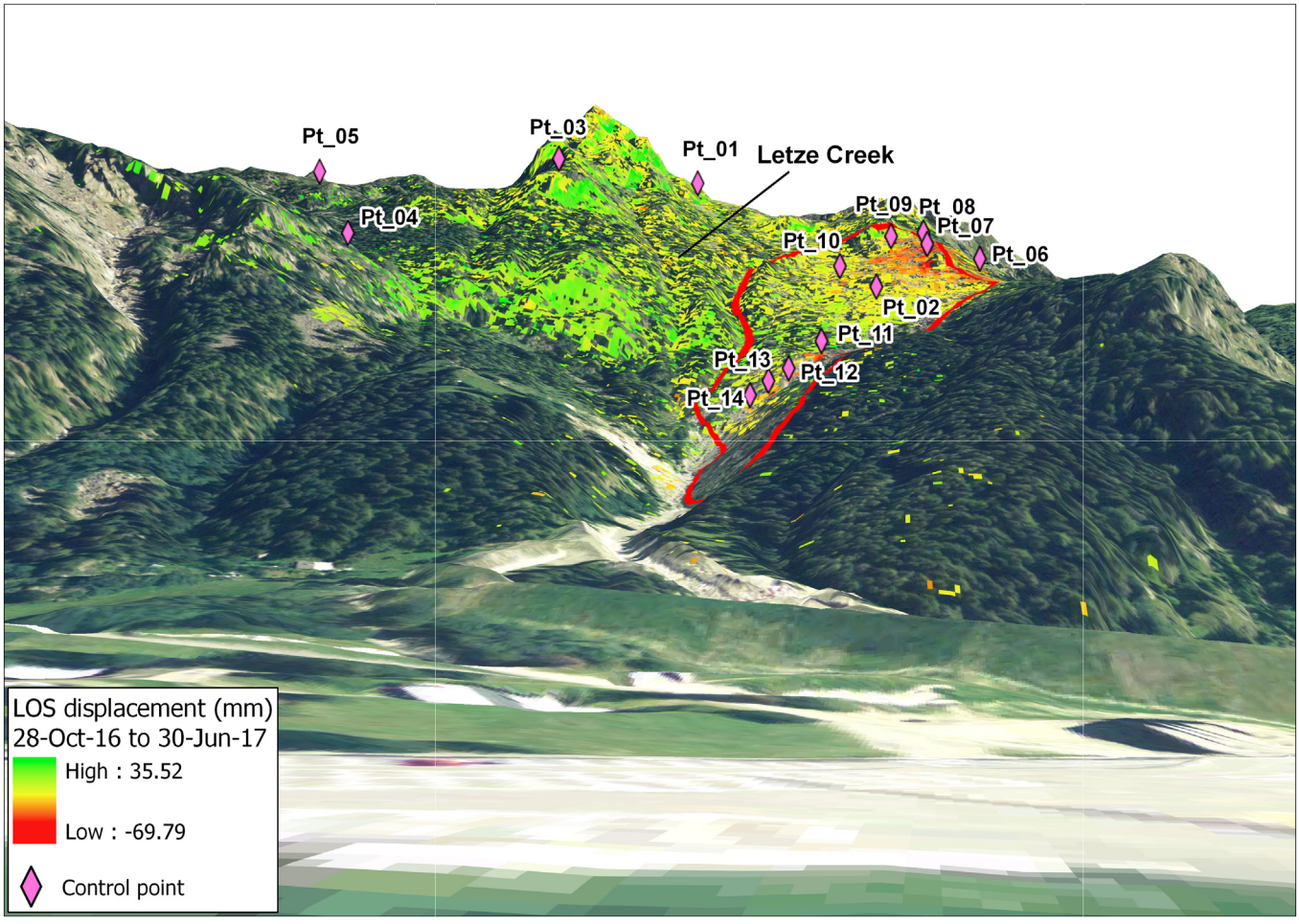

Fig. 12. Cumulative deformation map produced by the GBInSAR from 28 October 2016 to 30 June 2017, as seen from the looking perspective of the instrument. The red polygon includes the boundaries of the Bosmatto landslide, as well as the debris flow source area below the toe.

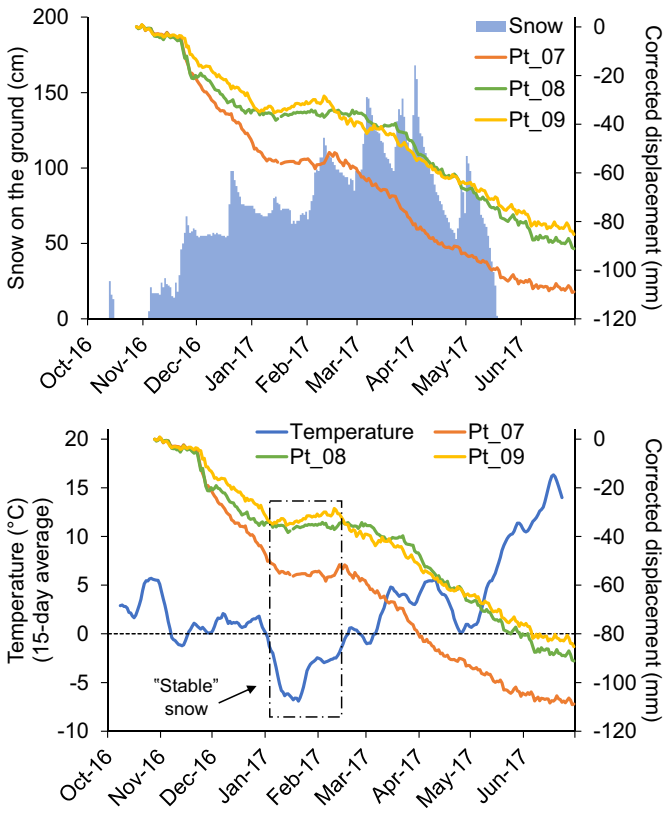

Fig. 13. Relationship between displacements measured by the GBInSAR at the head of the Bosmatto landslide and snow depth (top), and between displacements and a 15-day moving average of the daily air temperature (bottom). Displacements are corrected according to a 0.65 LOS sensitivity factor (Section 3.3).

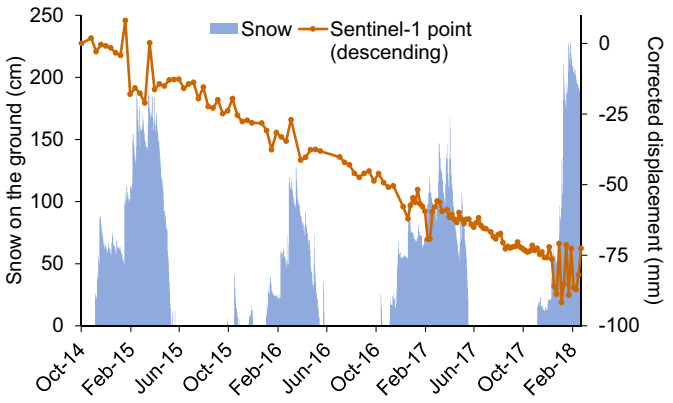

Fig. 14. Influence of snow depth on the variability of the displacements measured by Sentinel-1 during the winter seasons. Displacements are corrected according to a 0.9 LOS sensitivity factor (Section 3.2).

presence of a deep snow cover can have on measurement accuracy. Radar backscattering and the interferometric phase can be substantially altered depending on the employed wavelength and on the state of the snow on the ground. Snow surface melt, snow fall, and snow drift (due to gravity or to wind erosion and deposition) are all factors that can contribute to changing the propagation path of the incident microwave and lead to temporal decorrelation of the SAR signal (Rott et al., 2003). While such decorrelation may be corrected to a certain degree through specific processing tools, this is rarely considered in landslide applications. In general, penetration is best achieved under "stable" conditions of dry, cold, and homogeneous snow cover (Willatt et al., 2011).

In Fig. 13, the displacements of control points 07–09 (corrected according to a 0.65 LOS sensitivity factor, Section 3.3) are plotted in relation to the amount of snow on the ground and to the daily average air temperature. Meteorological data were collected at a weather station installed at 2100 m a.s.l. on the opposite side of the Lys Valley. Two phases of greater rate of displacement are observed: the first one beginning in mid−/late November, when snow depth rapidly grew over 50 cm; the second one in early February, when snow started to accumulate up to about 150 cm and then progressively melted away. A phase of essential absence of movement occurred in the midst of the winter season, during the month of January. This corresponds to a period of no significant variation of snow depth and of average daily temperatures well below zero, which presumably determined "stable" snow conditions. In the initial and last parts of the monitoring interval (up to mid-November 2016 and from mid-May 2017 onwards), when no snow cover (or a very thin one) was present on the ground, displacements measured by the GBInSAR are comparable with those measured by the GNSS and descending InSAR data. Yearly velocities extrapolated from such intervals are approximately 50–60 mm/y. These elements suggest that the GBInSAR mostly detected movements of the snow (i.e. depth variations and drift) that were not representative of the actual slope surface motion. An equivalent occurrence was described by Takahashi et al. (2013).

In dry snow conditions, the longer C-band (employed by the Sentinel-1 sensors) has a penetration depth of about 20 m, hence backscattering mostly stems from the ground surface (Schaffhauser et al., 2008). However, penetration depth drastically decreases to a few cm in case of wet snow. Snow fall and snow drift can also enhance the temporal decorrelation of the InSAR data (Rott et al., 2003). Fig. 14, showing the displacements of one of the descending targets within the Bosmatto landslide (corrected according to a 0.9 LOS sensitivity factor, Section 3.2), exemplifies the effect of temporal decorrelation typical of most PS/DS situated at high elevation in the study area. An evident variation of the data points around the main trend can be appreciated together with the accumulation of snow on the ground during each winter season. This variation appears to be more pronounced when snow depth is larger (see data points during the highly snowy 2017–2018 winter compared to the poorly snowy 2015–2016 winter). Still, coherence loss did not impact the quality of the displacement data in the long-term. PS/DS in the landslide area all showed a linear trend of movement, with velocities comparable to those depicted in Fig. 10 given the favorable LOS of the satellite in descending orbit.

4.2. Interpreted mechanism of the Bosmatto landslide through the combination of GNSS and decomposed Satellite InSAR data

In satellite InSAR monitoring, the availability of two different orbits of acquisition gives the opportunity to calculate the E-W and vertical components of the true movement vector; the horizontal component is thus underestimated since N-S movements cannot be extracted (Ferretti et al., 2007; Tofani et al., 2013; Ferretti, 2014). Nonetheless, the calculated easting component will provide an almost truthful estimation of the horizontal component in the case of nearly E-W planimetric movements of the slope, as it was assessed for the Bosmatto landslide based on GNSS monitoring (Fig. 7).

The procedure to decompose satellite InSAR data is as follows:

a) resampling of the PS/DS datasets by means of a regular grid;
b) identification of the grid elements that comprise at least one descending PS/DS and one ascending PS/DS (grid elements with yellow borders in Fig. 15);
c) for both orbits, averaging of all the PS/DS within each grid element to obtain a "synthetic target" (ST) characterized by a reference value of deformation in descending orbit and a reference value of deformation in ascending orbit;

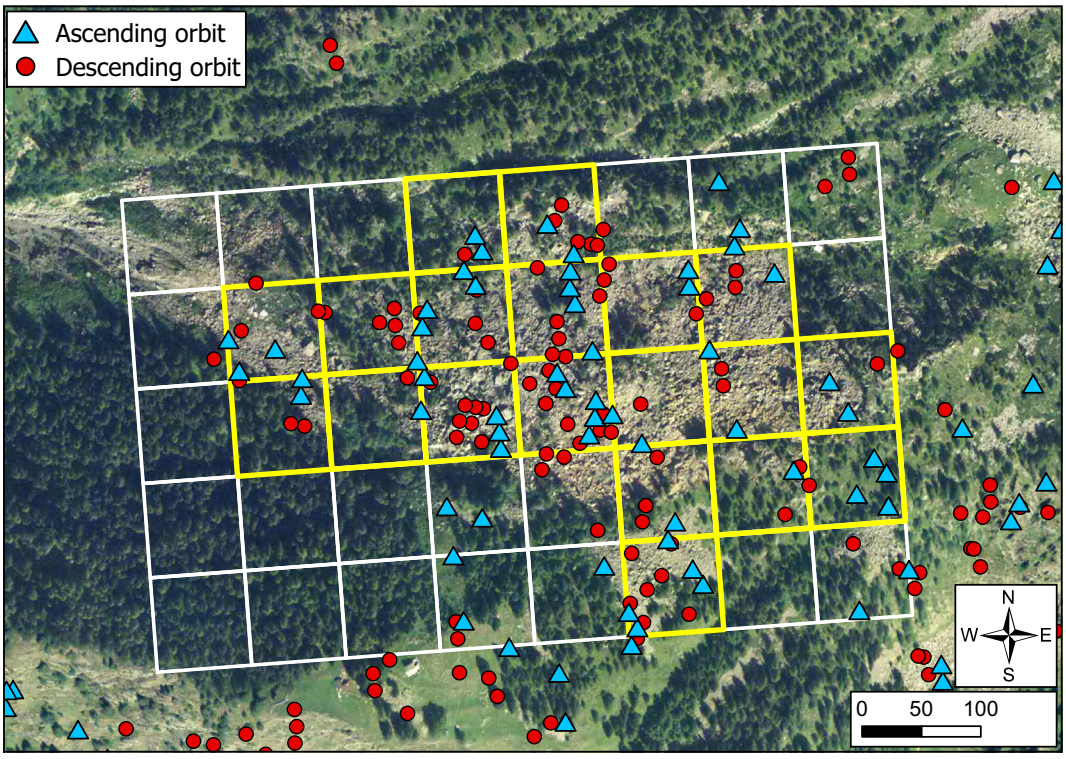

Fig. 15. Resampling of the satellite InSAR data by means of a 80 × 80 m grid for the calculation of the E-W and vertical components of movement.

d) values of deformation along the E-W and vertical components for each grid element are defined by a linear system of two equations:

$$\begin{cases} V_A = V_V\ cos(-\theta_A) + V_E\ sin(-\theta_A) \\ V_D = V_V\ \cos\theta_D + V_E\ \sin\theta_D \end{cases} \quad (1)$$

where V_A is the velocity in ascending orbit; V_D the velocity in descending orbit; V_E the easting velocity; V_V the vertical velocity; θ_A the LOS incidence angle in ascending orbit; and θ_D the LOS incidence angle in descending orbit.

In theory, resampling of the PS/DS data is not necessary if there are targets acting as "scatterers" in both orbits. In practice, that is extremely challenging when using medium resolution SAR sensors (Tofani et al., 2013; Ferretti, 2014). Resampling can also provide a more equal spatial distribution of the decomposed data. Here, this was accomplished by using a 80 × 80 m grid. Each ST was then associated to an approximated angle of dip according to:

$$\beta = \tan^{-1}(V_V/V_E) \quad (2)$$

where the dip angle β is overestimated proportionally to the underestimation of the horizontal component of movement.

The results of the decomposition procedure applied to the Bosmatto landslide are illustrated in Fig. 16. The landslide has comparable values of maximum vertical and E-W velocity (where negative E-W velocity means westward movement), ranging between 20 mm/y and 38.5 mm/y in the southeastern sector of the instability. Displacements at the toe are relatively greater in easting. The two deformation fields

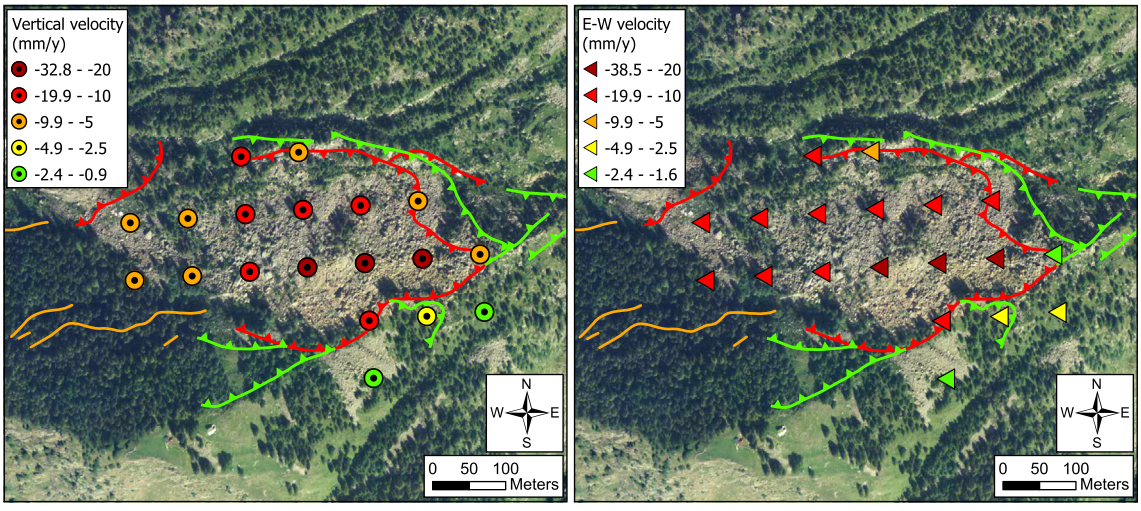

Fig. 16. Vertical (left) and E-W (right) velocity of the Bosmatto landslide derived from the decomposition of the satellite InSAR data. Negative E-W velocity means westward movement. See Fig. 4 for the meaning of the linear elements.

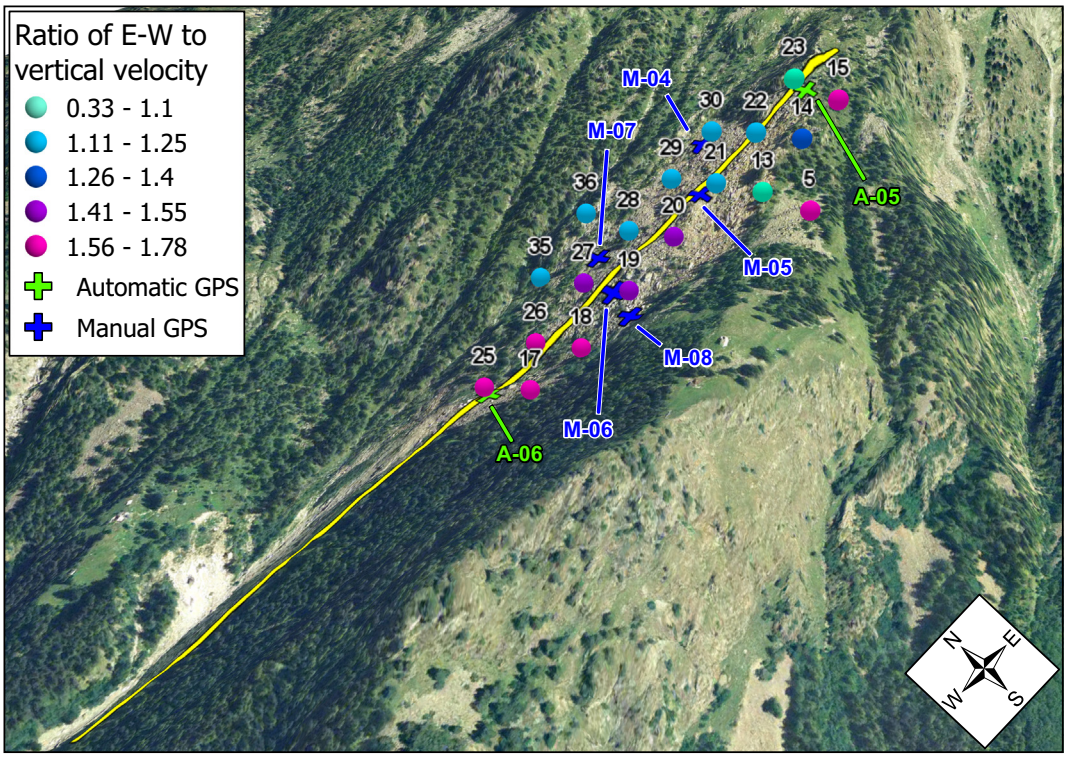

Fig. 17. Ratio of E-W to vertical velocity of the STs derived from the decomposition of the satellite InSAR data. Labels indicate the ID number assigned to each ST. The yellow line marks the trace of the cross-section in Fig. 18.

seem to have a similar distribution, as velocities in both components appear to decrease from head to toe.

In Fig. 17, further insights are gained by considering the ratio of E-W to vertical velocity (STs are labelled according to an ID number). The position of the GNSS stations is also highlighted. The yellow line, located between the two main rows of STs that run through the main landslide body (i.e. STs 17–22 and 25–30), marks the trace of the cross-section in Fig. 18. Such line intersects stations A-05, M-05, M-06, and A-06. The ratio of E-W to vertical velocity increases in the downslope direction, meaning that deformation along the horizontal component progressively becomes more predominant from head to toe.

This is made explicit in Fig. 18, where a vector is drawn for each measuring point intersected by the profile trace in Fig. 17. For satellite InSAR data, a vector represents the average of the pair of STs that is adjacent to the profile trace at the respective point along the slope. For GNSS stations for campaign measurements, vectors are calculated for the period 14 October 2010 to 8 November 2013, in order to not include the first years of acquisition (characterized by slightly larger velocities, Fig. 9) and to overlap the interval covered by the permanent GNSS stations.

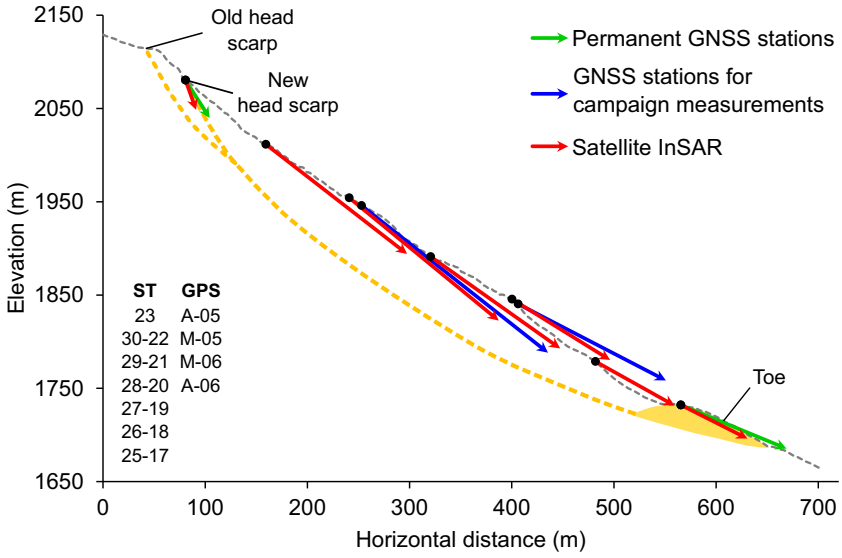

Fig. 18. Cross-section of the Bosmatto landslide resulting from the analysis of the movement vectors. The orange dashed line delineates the broadly roto-translational mechanism of the landslide, the orange shaded polygon the transition between the toe and the debris flow source area. In the lower left corner, IDs of the measuring points are listed in order from head to toe.

Vector length is proportional to the yearly 3D velocity, where for STs the E-W component is assumed equal to the total horizontal component. As expected, owing to the underestimation of the horizontal component, satellite InSAR data feature shorter vector lengths and higher dip angles with respect to their GNSS counterparts. Vectors in the head scarp area dip at a high angle into the slope, then gradually become sub-parallel to the slope surface further downslope, and ultimately slightly dip out of the slope in proximity of the toe. Deformation rates at the toe are of lower magnitude than in the upper parts of the landslide (stations A-05 and ST-23, situated on top of the new head scarp, may not be fully involved in the movement of the landslide). This element hints at the fact that undercutting of the toe by the Letze Creek is not the only destabilizing factor, as in such a case the largest deformation rates may be expected to occur in that sector.

Based on the analysis of the monitoring data, it is inferred that the Bosmatto landslide is a large rockslide that also involves deformation and shearing of the bedrock at depth. The gradual rotation of the dip angles of movement denotes that the instability translates in a generally coherent way according to a broadly roto-translational mechanism. At the toe, the basal shear surface likely coincides with the heavily brecciated layer identified at 30–40 m of depth in the borehole log (Fig. 5). The point of daylighting of this plane of weakness cannot be determined in the field because of the complex transition from landslide material to alluvial/debris flow deposits of the Letze Creek. Although the slope sector around the old head scarp is still included in the instability, activity is mostly concentrated downslope of the new head scarp. The lack of deep inclinometer measurements prevents from reaching a higher level of detail concerning the characteristics of the failure plane throughout the slope. The volume of the unstable mass is estimated at approximately $2.5 - 3.5 * 10^6$ m^3.

4.3. Implications for the monitoring of large landslides in high alpine environments

The combination of different monitoring techniques and an accurate analysis of the surface displacements can shed light on the basic features of large landslides in high alpine environments. The following considerations were drawn from the portrayed results.

Data from the GBInSAR monitoring campaign evidenced the sensitivity of the technique to the presence of "unstable" snow on the ground, especially to intervals of snow accumulation and melting. Without any other source of cross-validation, the greater displacement rates detected from February to May 2017 could be easily interpreted as a response of the slope to seasonal snow melting and consequent increase of pore water pressure. This relation has been found in several alpine rockslides, and in some cases rapid snow melt periods have been the final trigger of catastrophic rock avalanches (Sartori et al., 2003; Geertsema et al., 2006; Nishii et al., 2013; Crosta et al., 2014). However, no such behavior was observed in the satellite InSAR and permanent GNSS datasets (the low acquisition frequency at GNSS stations for campaign measurements would not allow for the detection of seasonal trends). These all indicate a long-term, steady-state slope creep, with average velocities that, including all the available GNSS data, range from <10 mm/y to >50 mm/y depending on the sector of the instability (Figs. 8–10).

The interaction between the sub-surface water circulation and the stability of the slope remains hard to define: if on one hand the October 2000 reactivation coincided with a phase of heavy rainfall, on the other it seems that the rockslide is not sensitive to variations of pore water pressure due to seasonality or ordinary precipitation. Subsequent rainstorms have not caused variations in landslide activity either. As no monitoring was being performed at the time, the specific conditions that caused the October 2000 reactivation cannot be safely determined at this stage.

The direction of movement of the Bosmatto landslide, according to which the easting component vastly defines the actual horizontal component, favored the integration of the GNSS and decomposed satellite InSAR records. Even if the two monitoring campaigns were undertaken over different time frames, the outcomes are nonetheless extremely similar. It can be deduced that the slope has been deforming at a basically constant rate for the last several years. In Table 1, the values of horizontal (or E-W) velocity, vertical velocity, 3D (or near-3D) velocity, and dip angle from the vectors in Fig. 18 are compared; GNSS stations and STs situated at roughly the same point along the cross-section are outlined with the same color. The parameters of stations M-04, M-07, and M-08 are reported as well. The targets present very small discrepancies in rates (<4 mm/y) along the vertical component, which can be fully derived from both GNSS and satellite InSAR monitoring. As expected, discrepancies between E-W velocities of the STs and horizontal velocities of the GNSS stations are slightly larger (up to 7.8 mm/y). Consequently, STs further underestimate the magnitude of the 3D vector (up to 9.1 mm/y) and overestimate the angle of dip by a maximum value of 12°. It should also be noted that discrepancies may be enhanced by the approximations intrinsic to the resampling procedure utilized to decompose the satellite InSAR data (Section 4.2).

Table 1
Parameters of slope deformation retrieved at GNSS stations and STs.

GNSS	Horizontal velocity (mm/y)	Vertical velocity (mm/y)	3D velocity (mm/y)	Dip (°)
A-05	−4.3	−7.4	8.6	60
A-06	−18.8	−8.5	20.7	24
M-04	−5.2	−6.5	8.3	51
M-05	−33.2	−28.8	44.0	41
M-06	−26.3	−14.9	30.2	30
M-07	−22.9	−9.5	24.8	23
M-08	−48.0	−20.4	52.2	23

ST	E-W velocity (mm/y)	Vertical velocity (mm/y)	Near-3D velocity (mm/y)	Dip (°)
23	−1.9	−5.8	6.1	72
22–30	−25.2	−21.4	33.0	40
21–29	−26.6	−24.0	35.8	42
20–28	−23.1	−17.9	29.2	38
19–27	−17.5	−11.9	21.1	34
18–26	−14.1	−8.6	16.5	31
17–25	−11.9	−7.2	13.9	31

Despite these limitations, the parameters of slope deformation retrieved at STs are remarkably similar to the ones measured at GNSS stations. This has potentially important implications for the monitoring of the Bosmatto landslide and of similar alpine rockslides, as satellite InSAR can usually guarantee improved spatial coverage and measurement accuracy, as well as systematic acquisitions suitable to regular monitoring applications since the launch of the Sentinel-1 constellation (Raspini et al., 2018). Still, conventional techniques such as topographic and GNSS surveying represent the essential monitoring tools during the winter months (when interferometric images may experience loss of coherence) and, most crucially, to retrieve the true movement vector in the case of instabilities affected by a significant northing component. Monitoring through permanent GNSS stations, featuring a temporal resolution of several acquisitions per day, may also be more suitable for detecting the onset of rapid accelerating trends.

5. Conclusions

The Bosmatto landslide, located on a steep alpine slope in the Northwestern Italian Alps, experienced a sudden reactivation on 15 October 2000. The event was triggered by a period of intense and prolonged rainfall, giving place to a destructive debris flow channeled down the narrow bed of the Letze Creek. The main body appears as a chaotic mass of large disjointed blocks and fragments of metamorphic bedrock within a scarce sandy to gravelly matrix. Over the years, investigations aimed at assessing the mechanism of the landslide had not brought to definitive conclusions.

The joint analysis of GNSS, satellite InSAR, and GBInSAR data, as a whole collected over a time span of 16 years, provided crucial insights into the mechanism and behavior of the landslide. In particular, the fundamental deformation field of the slope was validated from the combination of GNSS and decomposed satellite InSAR records. It was suggested that the Bosmatto landslide is a large rockslide that moves in a generally coherent way according to a broadly roto-translational mechanism. Shearing of the bedrock likely occurs at a depth of several tens of meters and, at least in the lower part of the landslide, exploits a heavily deformed weak zone composed of breccia and gauge layers (Fig. 5). This would yield a volume of the unstable mass of approximately $2.5 - 3.5 * 10^6$ m^3.

The landslide activity has been in the form of a steady-state creep for the last several years, with average velocities ranging from <10 mm/y to >50 mm/y. As the largest movements are in the head scarp area, undercutting by the Letze Creek was not deemed as the sole destabilizing factor. In this sense, the October 2000 debris flow and the erosion at the toe may be considered as processes that are only complementary to the slope stability issue at overall scale.

The work highlighted challenges and implications related to slope monitoring in high alpine environments. Ku-band GBInSAR acquisitions were heavily affected by the presence of snow on the mountain slope (Fig. 13). C-band Sentinel-1 acquisitions also showed variation of the data points around the main trend during the winter seasons, although long-term trends could still be appreciated (Fig. 14). STs, obtained from the decomposition of the ascending and descending satellite InSAR datasets, were remarkably consistent with the GNSS measurements, especially concerning movements along the vertical component (Table 1). This was favored by the nearly E-W direction of slope movement, which prevented a significant underestimation of the horizontal component. In light of the better spatial coverage and measurement accuracy, the satellite InSAR technique could therefore prove essential to enhance the monitoring of the Bosmatto landslide and of similar alpine rockslides.

References

Antonello, G., Casagli, N., Farina, P., Leva, D., Nico, G., Sieber, A.J., Tarchi, D., 2004. Ground-based SAR interferometry for monitoring mass movements. Landslides 1 (1), 21–28.

Bardi, F., Frodella, W., Ciampalini, A., Bianchini, S., Del Ventisette, C., Gigli, G., Fanti, R., Moretti, S., Basile, G., Casagli, N., 2014. Integration between ground based and satellite SAR data in landslide mapping: the San Fratello case study. Geomorphology 223, 45–60.

Barla, G., Antolini, F., Barla, M., Mensi, E., Piovano, G., 2010. Monitoring of the Beauregard landslide (Aosta Valley, Italy) using advanced and conventional techniques. Eng. Geol. 116 (3–4), 218–235.

Carlà, T., Farina, P., Intrieri, E., Ketizmen, H., Casagli, N., 2018. Integration of ground-based radar and satellite InSAR data for the analysis of an unexpected slope failure in an open-pit mine. Eng. Geol. 235, 39–52.

Casagli, N., Catani, F., Del Ventisette, C., Luzi, G., 2010. Monitoring, prediction, and early warning using ground-based radar interferometry. Landslides 7 (3), 291–301.

Colesanti, C., Wasowski, J., 2006. Investigating landslides with space-borne Synthetic Aperture Radar (SAR) interferometry. Eng. Geol. 88, 173–199.

Compagnoni, R., Dal Piaz, G.V., Hunziker, J.C., Gosso, G., Lombardo, B., Wiliams, P.F., 1977. The Sesia-Lanzo Zone: a slice of continental crust, with alpine HP–LT assemblages in the Western Italian Alps. Rend. Soc. Ital. Mineral. Petrol. 33, 281–334.

Crosta, G.B., di Prisco, C., Frattini, P., Frigerio, G., Castellanza, R., Agliardi, F., 2014. Chasing a complete understanding of the triggering mechanisms of a large rapidly evolving rockslide. Landslides 11 (5), 747–764.

Crosta, G.B., Agliardi, F., Rivolta, C., Alberti, S., Dei Cas, L., 2017. Long-term evolution and early warning strategies for complex rockslides by real-time monitoring. Landslides 14 (5), 1615–1632.

Dal Piaz, G.V., Hunziker, J.C., Martinotti, G., 1972. La Zona Sesia – Lanzo e l'evoluzione tettonico-metamorfica delle Alpi Nordoccidentali interne. Mem. Soc. Geol. Ital. 11, 433–460 (in Italian).

Del Ventisette, C., Casagli, N., Fortuny-Guasch, J., Tarchi, D., 2012. Ruinon landslide (Valfurva, Italy) activity in relation to rainfall by means of GBInSAR monitoring. Landslides 9 (4), 497–509.

Eberhardt, E., Watson, A.D., Loew, S., 2008. Improving the interpretation of slope monitoring and early warning data through better understanding of complex deep-seated landslide failure mechanisms. In: Chen, Z., Zhang, J., Li, Z., Wu, F., Ho, K. (Eds.), Landslides and Engineered Slopes: From the Past to the Future. Taylor & Francis, London, pp. 39–51.

Ferretti, A., 2014. Satellite InSAR Data: Reservoir Monitoring From Space. EAGE Publications, p. 159.

Ferretti, A., Savio, G., Barzaghi, R., Borghi, A., Musazzi, S., Novali, F., Prati, C., Rocca, F., 2007. Submillimeter accuracy of InSAR time series: experimental validation. IEEE Trans. Geosci. Remote Sens. 45 (5), 1142–1153.

Ferretti, A., Fumagalli, A., Novali, F., Prati, C., Rocca, F., Rucci, A., 2011. A new algorithm for processing interferometric data-stacks: SqueeSAR. IEEE Trans. Geosci. Remote Sens. 49 (9), 3460–3470.

Gaffet, S., Guglielmi, Y., Cappa, F., Pambrun, C., Monfret, T., Amitrano, D., 2010. Use of simultaneous seismic, GPS and meteorological monitoring for the characterization of a large unstable mountain slope in the southern French Alps. Geophys. J. Int. 182 (3), 1395–1410.

Geertsema, M., Hungr, O., Schwab, J.W., Evans, S.G., 2006. A large rockslide–debris avalanche in cohesive soil at Pink Mountain, northeastern British Columbia, Canada. Eng. Geol. 83 (1–2), 64–75.

Gischig, V.S., Moore, J.R., Evans, K.F., Amann, F., Loew, S., 2011. Thermomechanical forcing of deep rock slope deformation: 2. The Randa rock slope instability. J. Geophys. Res. Earth Surf. 116, F04011.

Gosso, G., 1977. Metamorphic evolution and fold history in the eclogitic micaschists of the upper Gressoney Valley (Sesia-Lanzo Zone, Western Alps). Rend. Soc. Ital. Mineral. Petrol. 33 (1), 389–407.

Helmstetter, A., Garambois, S., 2010. Seismic monitoring of Séchilienne rockslide (French Alps): analysis of seismic signals and their correlation with rainfalls. J. Geophys. Res. Earth Surf. 115, F03016.

Journalt, J., Macciotta, R., Hendry, M.T., Charbonneau, F., Huntley, D., Bobrowsky, P.T., 2018. Measuring displacements of the Thompson River valley landslides, south of Ashcroft, BC, Canada, using satellite InSAR. Landslides 15 (4), 621–636.

Leva, D., Nico, G., Tarchi, D., Fortuny-Guasch, J., Sieber, A.J., 2003. Temporal analysis of a landslide by means of a ground-based SAR interferometer. IEEE Trans. Geosci. Remote Sens. 41 (4), 745–752.

Luzi, G., Pieraccini, M., Mecatti, D., Noferini, L., Guidi, G., Moia, F., Atzeni, C., 2004. Ground-based radar interferometry for landslides monitoring: atmospheric and instrumental decorrelation sources on experimental data. IEEE Trans. Geosci. Remote Sens. 42 (11), 2454–2466.

Luzi, G., Pieraccini, M., Mecatti, D., Noferini, L., Macaluso, G., Galgaro, A., Atzeni, C., 2006. Advances in ground based microwave interferometry for landslide survey: a case study. Int. J. Remote Sens. 27 (12), 2331–2350.

Manconi, A., Kourkouli, P., Caduff, R., Strozzi, T., Loew, S., 2018. Monitoring surface deformation over a failing rock slope with the ESA Sentinels: insights from Moosfluh instability, Swiss Alps. Remote Sens. 10 (5), 672.

Marcato, G., Mantovani, M., Pasuto, A., Zabuski, L., Borgatti, L., 2012. Monitoring, numerical modelling and hazard mitigation of the Moscardo landslide (Eastern Italian Alps). Eng. Geol. 128, 95–107.

Nishii, R., Matsuoka, N., 2010. Monitoring rapid head scarp movement in an alpine rockslide. Eng. Geol. 115 (1–2), 49–57.

Nishii, R., Matsuoka, N., Daimaru, H., Yasuda, M., 2013. Precursors and triggers of an alpine rockslide in Japan: the 2004 partial collapse during a snow-melting period. Landslides 10 (1), 75–82.

Raspini, F., Bianchini, S., Ciampalini, A., Del Soldato, M., Solari, L., Novali, F., Del Conte, S., Rucci, A., Ferretti, A., Casagli, N., 2018. Continuous, semi-automatic monitoring of ground deformation using Sentinel-1 satellites. Sci. Rep. 8, 7253.

Rott, H., Nagler, T., Scheiber, R., 2003. Snow mass retrieval by means of SAR interferometry. Proceedings of FRINGE 2003 Workshop. Frascati, Italy, 1–5 December 2003, pp. 1–6.

Sartori, M., Baillifard, F., Jaboyedoff, M., Rouiller, J.-D., 2003. Kinematics of the 1991 Randa rockslides (Valais, Switzerland). Nat. Hazards Earth Syst. Sci. 3 (5), 423–433.

Schaffhauser, A., Adams, M., Fromm, R., Jörg, P., Luzi, G., Noferini, L., Sailer, R., 2008. Remote sensing based retrieval of snow cover properties. Cold Reg. Sci. Technol. 54, 164–175.

Strozzi, T., Farina, P., Corsini, A., Ambrosi, C., Thüring, M., Zilger, J., Wiesmann, A., Wegmüller, U., Werner, C., 2005. Survey and monitoring of landslide displacements by means of L-band satellite SAR interferometry. Landslides 2 (3), 193–201.

Takahashi, K., Matsumoto, M., Sato, M., 2013. Continuous observation of natural-disaster-affeted areas using ground-based SAR interferometry. IEEE J. Sel. Topics Appl. Earth Observ. Remote Sens. 6 (3), 1286–1294.

Tarchi, D., Casagli, N., Fanti, R., Leva, D., Luzi, G., Pasuto, A., Pieraccini, M., Silvano, S., 2003. Landslide monitoring by using ground-based SAR interferometry: an example of application to the Tessina landslide in Italy. Eng. Geol. 68 (1–2), 15–30.

Tessari, G., Floris, M., Pasquali, P., 2017. Phase and amplitude analyses of SAR data for landslide detection and monitoring in non-urban areas located in the North-Eastern Italian pre-Alps. Environ. Earth Sci. 76 (2), 85.

Tofani, V., Raspini, F., Catani, F., Casagli, N., 2013. Persistent Scatterer Interferometry (PSI) technique for landslide characterization and monitoring. Remote Sens. 5, 1045–1065.

Willatt, R., Laxon, S., Giles, K., Cullen, R., Haas, C., Helm, V., 2011. Ku-band radar penetration into snow cover on Arctic sea ice using airborne data. Ann. Glaciol. 52 (57), 197–205.

Zucali, M., Spalla, M.I., 2011. Prograde lawsonite during the flow of continental crust in the Alpine subduction: strain vs. metamorphism partitioning, a field-analysis approach to inter tectonometamorphic evolutions (Sesia-Lanzo Zone, Western Italian Alps). J. Struct. Geol. 33, 381–398.

Zucali, M., Spalla, M.I., Gosso, G., 2002. Strain partitioning and fabric evolution as a correlation tool: the example of the Eclogitic Micaschists Complex in the Sesia-Lanzo Zone (Monte Mucrone-Monte Mars, Western Alps, Italy). Schweiz. Mineral. Petrogr. Mitt. 82, 429–454.